Available online at www.sciencedirect.com
ScienceDirect
International Journal of Heat and Mass Transfer 51 (2008) 2494–2505
International Journal of HEAT and MASS TRANSFER
www.elsevier.com/locate/ijhmt

A porous medium analogy for the helium flow in CICCs

L. Bottura [a,*], C. Marinucci [b]

[a] CERN, M26210, CH-1211 Geneva, Switzerland
[b] EPFL/CRPP, Fusion Technology Division, CH-5232 Villigen PSI, Switzerland

Received 5 December 2006; received in revised form 30 July 2007
Available online 23 October 2007

Abstract

Cable-in-Conduits are superconducting conductors that consist of a bundle of cabled strands enclosed in a leak-tight pipe, the jacket. Helium flows inside the jacket, in a meandrous flow path defined by the intersticial space among the cabled strands, or in specific passages introduced by design to reduce pressure drop. The main advantage of this design is to bring the coolant in close thermal contact with the superconductor, thus enhancing the heat removal as well as its thermal stability. To date, however, the details of the flow and heat transfer mechanism in this complex geometry are not well understood. We propose to use an analogy between the bundle of strands in the cable and a porous media. The analogy provides simple correlations for pressure drop and heat transfer prediction that contain explicitly permeability, drag factor and thermal dispersion. We use published pressure drop data to show that the range of permeability of a CICC is within the expected values for a porous medium with the same equivalent particle diameter, while the drag factor is consistently lower than what expected from the theory of particle beds, which will require further work to produce a satisfactory explanation. Experimental data for the internal heat transfer obtained from a short ITER conductor sample are in good agreement with the expected contribution of thermal dispersion, which supports or proposal.

Keywords: Cable-in-Conduit conductors; Heat transfer; Permeability; Porous media; Pressure drop; Thermal dispersion

1. Introduction

Cable-in-Conduit conductors (in short CICCs) consist of a bundle of superconducting strands cabled in various configurations and size, depending on the desired current carrying capacity, and enclosed in a leak-tight conduit (also called the *jacket*). In most of the applications to date, CICCs are cooled by internal convection, by a flow of liquid or supercritical helium. The helium flows among the strands, in the interstices of the cable, along tortuous and irregular paths. Various CICC configurations have been designed, produced and tested since the concept was first proposed more than 30 years ago by Hoenig et al. at MIT [1,2]. We show in Fig. 1 the original schematics of the CICC proposals, as well as some of the late realisations for the CICCs of ITER [3] and Wendelstein-7X [4]. In some configurations (see the ITER example in Fig. 1), additional channels have been added using pipes within the cable, wraps and spacers, spirals in the center of the cable, or co-laminated pipes to provide a low hydraulic impedance flow path. The typical size of the strands ranges from 0.5 to 1 mm. The cables are formed by twisting or braiding in multiple stages a number of strands ranging from 100 to 1000, depending on the required current carrying capacity. The cable must be compacted to achieve a mechanically stable configuration, still limiting the strand deformation. As a result the feasible range of void fraction in the cable (the ratio of void space to the total cable area) extends from 0.25 to 0.45. The final diameter of the cable ranges from about 10 mm for small cables (Fig. 1, bottom left), to about 50 mm for large size cables used in ITER (Fig. 1, bottom right).

The advantage, and indeed the main reason of the CICC design, is that the thermal vector, the flowing helium, is in intimate contact with the superconducting strands. Thanks

* Corresponding author. Tel.: +41 22 767 3729; fax: +41 22 767 6230.
E-mail address: Luca.Bottura@cern.ch (L. Bottura).

0017-9310/$ - see front matter © 2007 Elsevier Ltd. All rights reserved.
doi:10.1016/j.ijheatmasstransfer.2007.07.051

Nomenclature

List of symbols

A_S	solid phase cross section
A_F	fluid phase cross section
c_{pF}	fluid specific heat at constant pressure
C_F	drag coefficient
D_h	hydraulic diameter
D_{strand}	strand diameter
$D_{particle}$	particle diameter, equivalent diameter of a spherical particle
f_{dead}	dead space in the porous matrix (sealed pores)
f	friction factor
h	heat transfer coefficient
k	effective thermal conductivity
k_F	fluid molecular thermal conductivity
k_L	effective thermal conductivity in the direction of the flow
k_T	effective thermal conductivity in the direction transverse to the flow
K	permeability
Nu	Nusselt number
Nu_φ	seepage Nusselt number
p	fluid pressure
p_w	wetted perimeter
Pe_φ	seepage Peclet number
Pr	Prandtl number
Re	Reynolds number
Re_φ	seepage Reynolds number
S	surface per unit volume of the solid phase
T	fluid temperature
v	average fluid velocity in the pores
v_φ	seepage velocity
α_F	fluid diffusivity
φ	porosity, identical to void fraction
μ	viscosity
ρ_F	fluid density
θ	average cabling angle

to this, CICCs have the best possible local cooling conditions and achieve the highest expected stability against thermal perturbations [5]. The superior stability makes the CICC concept attractive for applications such as thermonuclear fusion, where the electromagnetic and nuclear environment cause relatively high DC and transient thermal loading of the superconducting coil. Cooling and stability have often been a design driver in the layout of a CICC as well as magnets wound with it.

This leads us finally to one of the main difficulties in CICC design, namely the precise knowledge of the thermo-hydraulics of the flow and in particular pressure drop and heat transfer characteristics. This problem is particularly relevant in the presence of parallel flow paths in

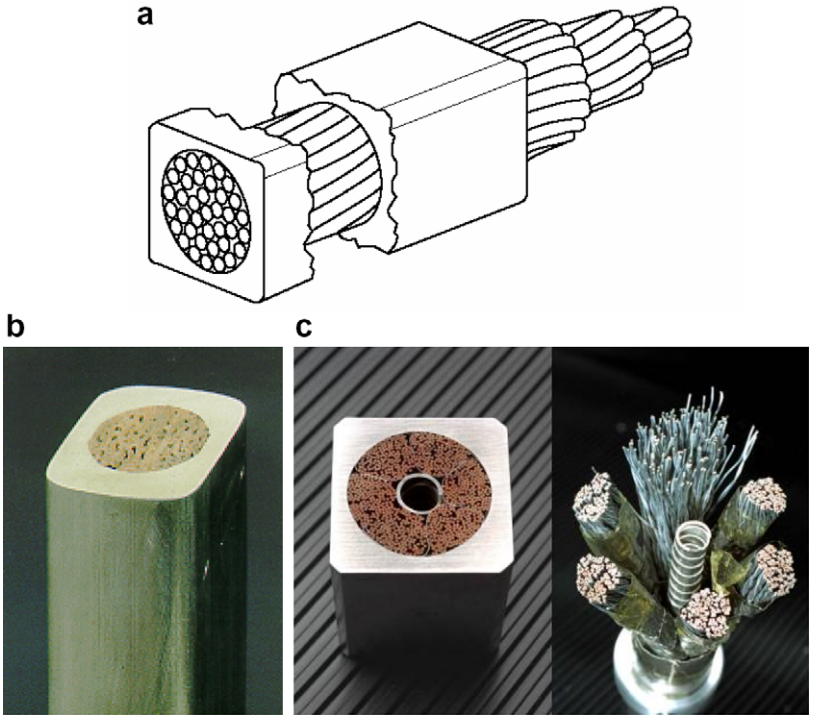

Fig. 1. The concept of a CICC (top, reproduced from [2]), and some recent realisation of CICC's for fusion magnets: the Wendelstein-7X conductor [4] (bottom left) and an ITER prototype [3] (bottom center and right).

the cable cross section, as is the case of the ITER CICC, in which case the overall cooling efficiency depends on the heat transfer between the helium in the cable interstices, nearly stagnant, and the helium in the channel, flowing at relatively high speed.

Research so far has focussed on adapting known correlations for pipe flow, using hydraulic analogy and average values of the flow cross section and hydraulic diameter. The adapted correlations have been used to interpret measurements of pressure drop and heat convection. The result of this work is only marginally satisfactory for design purposes, and the uncertainty in the values used for the heat transfer is compensated by design safety factors. Indeed, we feel that this approach has reached its limit for the understanding of the physical phenomena involved.

It is for this reason that we propose to consider the cable cross section of the CICCs shown in Fig. 1 as a porous medium, for which we can use established theory and a large amount of data in the literature. The cabled strands form the packed solid phase that obstructs the free flow in the channel. The pores are the interstices between strands, and the coolant flows in the tortuous path connecting the interstices. In this paper we discuss the implications of this analogy, based on the known theory of mass, momentum and energy convection in porous media (see for example [6] and references therein).

Before we start our discussion, we recall that a similar approach was already considered by others. Long [7] went into extensive details to obtain friction factor and heat transfer correlations that apply to ITER-like CICCs. The resulting theory is noteworthy, but unfortunately it contains a large number of unknown parameters that depend on the microscopic and macroscopic characteristic of the CICC. For this reason it is difficult to interpret, especially to evidence parametric dependencies on the main design quantities such as strand diameter, void fraction, or cooling massflow. Within the scope of his research, Long reviewed available pressure drop data and derived permeability and drag coefficients that we will discuss later. Renard [8] used the theory of porous media for the pressure drop in the cable, but discarded its use in a range of Reynolds number larger than 10, preferring the experimental fit of Katheder [9]. His focus was on the flow in the central cooling channel of ITER-like CICCs, and he did not pursue the analogy. Wang et al. [10] developed a model for the quench propagation in the HT-7U CICC coils that considers the flow of helium as porous. They used given permeability and drag coefficient values to predict the pressure drop, but neglected the effect of thermal dispersion, that we discuss later. Finally, Zanino and Savoldi Richard [11] used the Darcy–Forcheimer form of the momentum balance to derive permeability and drag coefficient data from a series of CICCs tested over the past 10 years. They concluded that although some regularity could be found, both permeability and drag coefficient were strongly dependent on the details of the cable geometry, and that proper use of the analogy would require *a priori* determination of both parameters, which was judged beyond present capability. In their work they further hinted that heat transfer between strands and helium should be best predicted using porous media correlations.

In this paper we will develop these ideas, maintaining the discussion as simple as possible, and restricting to the main results that can be derived from a theory of convection in porous media relevant to forced flow in CICCs. We start with a brief introduction on transport phenomena in porous media. Next, we consider pressure drop, and we give estimates for permeability and drag coefficient appropriate to CICCs. We then review simple expressions for thermal dispersion, that results in a great increase of effective fluid conductivity under strong convection. The results are useful to explain enhanced heat transfer coefficients to the solid phase in the fluid flow (i.e., the cable) and the pipe wall delimiting the flow (i.e., the conduit). Finally, we conclude showing how the analogy can be used to interpret data taken during a heat pulse propagation experiment in a short length sample of a fusion CICC.

2. Definitions and conservation balances

In the most common configuration, the cable of a CICC is wound using N strands with a single diameter D_{strand}. When the average cabling angle θ is small, i.e., when $\cos\theta$ is close to one, the wetted perimeter of the cable is

$$p_{\mathrm{w}} \approx \frac{f_{\mathrm{dead}} N \pi D_{\mathrm{strand}}}{\cos\theta} \tag{1}$$

where the factor f_{dead} corrects the geometric wetted perimeter for the dead space enclosed between deformed strands [12]. The range of values for f_{dead} spans from 0.6, for tightly compacted cables, to 0.9 for loose cables.

The cross sections of the solid phase (strands) and of the fluid (helium) are:

$$A_{\mathrm{S}} = \frac{1}{\cos\theta} N \frac{\pi}{4} D_{\mathrm{strand}}^2 \tag{2}$$

$$A_{\mathrm{F}} = \frac{\varphi}{1-\varphi} \frac{1}{\cos\theta} N \frac{\pi}{4} D_{\mathrm{strand}}^2 \tag{3}$$

where φ is the void fraction of the cable. For pressure drop and heat transfer calculations we define an hydraulic diameter, computed using the standard definition for pipes:

$$D_{\mathrm{h}} = \frac{4A_{\mathrm{F}}}{p_{\mathrm{w}}} = \frac{\varphi}{1-\varphi} \frac{D_{\mathrm{strand}}}{f_{\mathrm{dead}}} \tag{4}$$

Conversely, a porous media is defined macroscopically by its porosity, i.e., the fraction of the total volume occupied by void and free to the flow. This corresponds to the void fraction φ of the superconducting cable in a CICC. The complement to one, $1-\varphi$, is the fraction of the solid phase in the medium, i.e., the strand fraction. The second macroscopic characteristic is the geometry of the solid phase (e.g. spheres, wires, and particles), which determines the flow and heat transfer properties, as discussed below. A large number of transport experiments in porous media are per-

formed on beds of packed particles of more or less uniform, spherical geometry. The superconducting cable of interest to us resembles rather a woven fiber or a bed of packed wires. To be able to use the existing results on beds of packed particles, we define an *equivalent particle diameter* D_{particle} that would result in the same solid surface per unit volume S as the CICC geometry [13]. D_{particle} is given by:

$$D_{\mathrm{particle}} = \frac{6}{S} \tag{5}$$

Using the expressions for the wetted perimeter and cross section of the cable given above (Eqs. (1) and (3)), we have that:

$$S = \frac{4 f_{\mathrm{dead}}}{D_{\mathrm{strand}}} \tag{6}$$

and by consequence:

$$D_{\mathrm{particle}} = \frac{3}{2 f_{\mathrm{dead}}} D_{\mathrm{strand}} \tag{7}$$

Different definitions of fluid velocity apply in porous media, corresponding to different length scales. At the first level, at a microscopic scale much larger than the molecular length, we define the *intrinsic* velocity of the fluid $\mathbf{V}$, that can be different from point to point within a pore. This is the velocity that describes the 3-D flow field within a pore.

The equations of flow are written for the *average* fluid velocity, $\mathbf{v}$, which is obtained averaging the intrinsic velocity $\mathbf{V}$ over a representative elementary volume of fluid V_{F} that excludes the solid phase, and whose size is large enough to produce a values independent on the volume itself. In practice V_{F} must be larger than the pore size, but smaller than the length scale of the macroscopic flow domain. This is the velocity commonly used to model flow and heat exchange in the long cooling channels of a CICC coil [5].

The balances of mass, momentum and energy require finally dealing with averages over a volume V of size comparable to V_{F}, but including both fluid and solid phases. The result of this averaging process produces fluid quantities, including the *seepage* velocity $\mathbf{v}_\varphi$, that are weighted by the porosity φ. The seepage velocity is related to the average fluid velocity $\mathbf{v}$ by:

$$\mathbf{v}_\varphi = \varphi \mathbf{v} \tag{8}$$

In the range of cooling conditions of interest here, the steady-state mass, momentum and energy conservation balances of the fluid in a porous medium are the following:

$$\varphi \frac{\partial \rho_{\mathrm{F}}}{\partial t} + \nabla(\rho \mathbf{v}_\varphi) = 0 \tag{9}$$

$$\nabla p = -\frac{\mu}{K}\mathbf{v}_\varphi - C_{\mathrm{F}} \frac{\rho_{\mathrm{F}}}{K^{1/2}} |\mathbf{v}_\varphi| \mathbf{v}_\varphi \tag{10}$$

$$\varphi \rho_{\mathrm{F}} c_{\mathrm{pF}} \frac{\partial T}{\partial t} + \rho_{\mathrm{F}} c_{\mathrm{pF}} \mathbf{v}_\varphi \nabla T = \varphi \nabla \cdot (k \nabla T) + \varphi \dot{q}'''_{\mathrm{F}} \tag{11}$$

whose derivation and discussion can be found in [6]. In the equations above C_{F} is a dimensionless drag coefficient, K the permeability (assumed to be isotropic), c_{pF} the fluid specific heat at constant pressure, k is an effective heat conductivity, and the other symbols are standard and defined in the list of symbols.

The second equation, Eq. (10), is the momentum balance in the form of the Dupuit–Forcheimer modification to the Darcy's equation for the gradient of pressure [6]. This equation neglects inertial effects in the fluid, and hence does not contain any time derivative. As discussed by Dresner in [14] and Shajii and Freidberg in [15], this approximation is applicable in the case of a CICC where friction is the dominating force opposing the pressure gradient. The first term in Eq. (10) is the low-speed linear drag relation established by Darcy, and the second term, often referred to as Forcheimer term, was established in the form presented above by Ward [16].

The energy balance, Eq. (11), applies to the case of incompressible fluid and neglecting the work performed by viscous forces. We retain this approximation for simplicity, although it is not essential to the discussion in this paper. The heat source $\dot{q}'''_{\mathrm{F}}$ includes all terms, and in particular heat transfer from the solid phase through the solid–fluid heat transfer coefficient. The heat conductivity k that appears in the diffusion flux is in general a tensor quantity that contains two contributions, namely the classical conductivity of the fluid k_{F} due to diffusion at the molecular scale, and an additional enhancement term due to flow mixing at the length scale of the pores. This second mechanism is the *thermal dispersion* peculiar to forced convection in porous media, and arises as the direct consequence of the tortuous flow path.

The non-dimensional numbers, used for the pressure drop and heat transfer correlations of forced flow in porous media, are the Prandtl, Reynolds, Nusselt, and Peclet numbers of the seepage flow, referred to the equivalent particle diameter:

$$Pr = \frac{\mu c_{\mathrm{pF}}}{k_{\mathrm{F}}} \tag{12}$$

$$Re_\varphi = \frac{\rho_{\mathrm{F}} v_\varphi D_{\mathrm{particle}}}{\mu} \tag{13}$$

$$Nu_\varphi = \frac{h D_{\mathrm{particle}}}{k_{\mathrm{F}}} \tag{14}$$

$$Pe_\varphi = \frac{v_\varphi D_{\mathrm{particle}}}{\alpha_{\mathrm{F}}} \tag{15}$$

In Eq. (15) α_{F} is the thermal diffusivity of the fluid, or:

$$\alpha_{\mathrm{F}} = \frac{k_{\mathrm{F}}}{\rho_{\mathrm{F}} c_{\mathrm{pF}}} \tag{16}$$

All CICC correlations, on the other hand, have been established using the average flow velocity in the cable, v, and the hydraulic diameter of the flow, D_{h}. They are hence dependent on a Reynolds number given by:

$$Re = \frac{\rho_F v D_h}{\mu} = \frac{2}{3}\frac{1}{1-\varphi} Re_\varphi \tag{17}$$

while the heat transfer correlations produce Nusselt numbers:

$$Nu = \frac{h D_h}{k_F} = \frac{2}{3}\frac{\varphi}{1-\varphi} Nu_\varphi \tag{18}$$

3. Pressure drop in a CICC vs. porous media

The hydraulic resistance that governs the pressure drop necessary to achieve a desired helium flow is one of the design issues in the thermal design of a CICC, and was identified already in early optimisation studies, such as that in [17]. As a basis of comparison, we define the friction factor f given by:

$$\frac{\partial p}{\partial x} = -2\frac{f}{D_h}\rho_F |v| v \tag{19}$$

where D_h is the hydraulic diameter of the flow. In this form, pressure drop data have been modelled by Katheder using the following correlation [9]:

$$f_{\text{Katheder}} = \frac{1}{4\varphi^{0.72}}\left(0.051 + \frac{19.5}{Re^{0.88}}\right) \tag{20}$$

The above expression is used extensively in the design and analysis of coils built with CICCs, but has been shown to have limited predictive capability and a large uncertainty, up to a factor 2 [11].

If we consider the CICC as a porous medium, we take Eq. (10) for a single component of the flow (e.g. the x direction), and we make use of the definitions given earlier, it is possible to identify terms in the momentum balance Eqs. (10) and (19), leading to the following friction factor:

$$f = \varphi^2 C_F \frac{D_h}{2K^{1/2}} + \varphi \frac{D_h^2}{2K}\frac{1}{Re} \tag{21}$$

which is a direct consequence of the Darcy–Forcheimer equation, and, so far, does not contain any free parameters. Comparing the expression above (Eq. (21)) to the fit of Katheder (Eq. (20)), we see that the dependence on the Reynolds number is very similar. On the other hand, the porosity appears explicitly in Eqs. (20) and (21) with a very different dependence, which is an interesting result and requires some explanation. In fact, as discussed later, also K and C_F depend on porosity, so that the whole scaling of f with φ is not trivial.

In Eq. (21) all parameters are known or can be computed from the cable geometry and operating conditions, apart for the permeability K and the drag coefficient C_F. These last are known to depend not only on the porosity, but also on the details of the geometry of the solid phase of the porous medium, i.e., the arrangement of the strands in the cable. Indeed, their determination for each geometric configuration and porosity is a long-standing problem, which is the main issue in the porous media analogy.

The reference value often quoted for the permeability is the following, obtained in the case of a packed bed of spherical particles of diameter D_{particle}, attributed to Carman–Kozeny:

$$K = \frac{D_{\text{particle}}^2 \varphi^3}{180(1-\varphi)^2} \tag{22}$$

In practice, it is known that the value of K can vary by orders of magnitude depending on the details of the pores and solid phase. Measurements and numerical simulations of porous flow in beds of fibers have shown that the value obtained from Eq. (22) may be too small [18–20]. Kaviany reports a small modification of the above expression [18]:

$$K = \frac{D_{\text{particle}}^2 \varphi^3}{150(1-\varphi)^2} \tag{23}$$

where the only difference is in the numerical factor at the denominator.

For the drag coefficient C_F, the values often quoted in the literature for beds of round particles are in the range of 0.5 for a porosity of 0.4. Kaviany reports the following dependency on the porosity [18]:

$$C_F = \frac{1.75}{\sqrt{150}\varphi^{3/2}} \tag{24}$$

Substituting the values of Eqs. (23) and (24) for permeability and drag coefficient in Eq. (21), we obtain the Ergun equation [21] in the following form that is directly comparable to the CICC fit of Katheder:

$$f = \frac{7}{12} + \frac{100}{3}\frac{1}{Re} \tag{25}$$

Eq. (25) has been verified experimentally and adapted using measured data. As an example, Achenbach [22] proposes the following correlation for packed beds of spherical particles, expressed again using the friction factor definition of Eq. (19):

$$f = \left(\frac{2}{3}\right)^{0.1}\frac{1}{Re^{0.1}} + \frac{320}{9}\frac{1}{Re} \tag{26}$$

In addition to the above configurations, we have selected for comparison the results obtained by Wu et al. on woven metal screens of different porosity and weaving pattern [23]. The correlations found are in a general form:

$$f = \frac{a}{Re} + \frac{b}{Re^c} \tag{27}$$

Suitable values of the fitting constants in the range $10 < Re < 1000$ vary from:

$a = 55.6$

$b = 0.55$

$c = 0.071$

for plain square woven screens, to:

$$a = 24.7$$
$$b = 0.99$$
$$c = 0.071$$

for twilled dutch woven screens.

The values obtained using the above correlations for packed bed of particles and woven screens, Eqs. (25)–(27), have been plotted in Fig. 2 for comparison to the CICC correlation of Katheder, Eq. (20) evaluated at a porosity of 0.35, which is typical of CICC's. At all Reynolds number the pressure drop predicted for the CICC is lower than in a bed of equivalent particles. We believe that this low value can be explained considering that while packed beds of particles and woven screens produce a solid phase with random structure, the strands are twisted repeatedly to form the cable of the CICC and produce a pattern of free channels with length much larger than the strand dimension, hence favouring the flow and reducing the pressure drop.

At low Reynolds ($Re < 100$) the values of the friction factor are lower but comparable to that of a packed bed of equivalent particles. This implies that for a CICC the values of permeability, the dominating friction mechanism at low Re, are comparable to those of a porous medium of same equivalent particle diameter. On the other hand, at high Reynolds ($Re > 1000$) the friction factor of a CICC is an order of magnitude smaller than that of a packed bed of particles and woven metal screens. We hence expect the drag coefficient, determining the high Re behaviour, to be much smaller in a CICC than in a porous medium of same equivalent particle diameter. This can be appreciated by computing the values of permeability K and drag coefficient C_F such that the friction factor obtained from the Darcy–Forcheimer equation (Eq. (21)) matches the empirical fit of Katheder (Eq. (20)). We obtain that the permeability of a CICC cabled with 0.8 mm strands and porosity 0.35 is of the order of 3.5×10^{-9} (m^2), to be compared to 1.2×10^{-9} (m^2) estimated using Eq. (22), i.e., a factor 3 higher. The drag coefficient of the same CICC is 0.055, to be compared to 0.65 obtained using Eq. (24), i.e., an order of magnitude smaller.

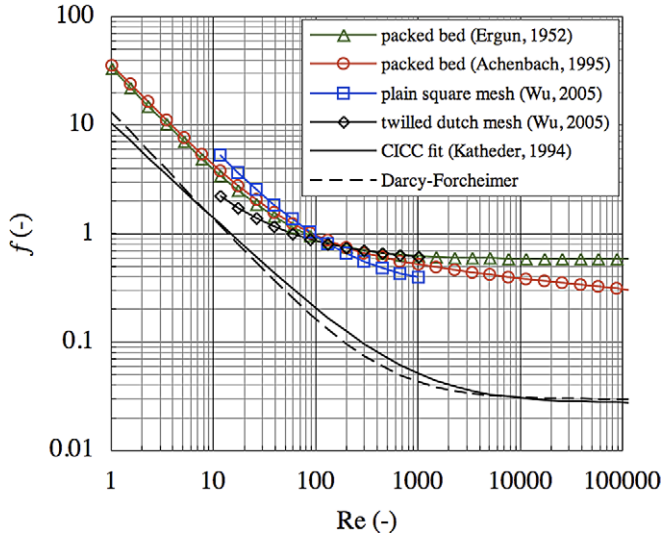

Fig. 2. Comparison of friction factor, as defined in Eq. (19), for packed beds (Ergun [21] and Achenbach [22]) woven metal screens (Wu et al. [23]) and typical CICC with a void fraction of 35% (Katheder [9]). The Darcy–Forcheimer Eq. (21) has been fitted to the CICC correlation using values of $K = 3.5 \times 10^{-9}$ (m^2) and $C_F = 0.055$.

In summary, the pressure drop of a CICC could be described well using the porous media momentum balance Eq. (10), or the friction factor Eq. (21), provided that the permeability and drag coefficient are known. These, in turn, appear to deviate from the theory of particle beds and woven fibers. The applicable range of values for the permeability and the drag coefficient of a CICC, and in particular their dependence on porosity, is the topic of the following section.

4. Permeability and drag coefficient estimates for CICCs

Permeability and drag coefficient are not known *a priori* for the complex configuration of the multi-stage cable in the CICC. Lacking an analytical basis, we have decided to resort on friction factors measured in CICCs of various size, built with strands of different diameter (from 0.6 to 1 mm), void fraction (from 25% to 47%), and cabling pattern, to form a data base of fitted K and C_F. A survey of data from the early CICC developments is reported in [7], while [11] gives some recent results on ITER CICCs. In addition to these data, we have used the measurements performed by Bagnasco et al. [24] on two small-size CICCs compacted at various void fraction from 35% to 25%. Permeability and drag coefficient can be extracted from friction factor data as described in [7], fitting the data with a model $f = a + b/Re$.

In Fig. 3 we have compiled the values of normalised permeability, defined as the ratio of $\frac{K}{D^2_{\text{particle}}}$, plotted as a function of porosity. In the same plot we have also reported the value predicted by Eq. (23), and the best fit using a model:

$$\frac{K}{D^2_{\text{particle}}} = \frac{\varphi^3}{A(1-\varphi)^2} \tag{28}$$

The dependence of the permeability on porosity is relatively clear and is consistent with the theoretical expectation. The minimum fit residual is obtained for $A = 140$ which is very close to the expected value $A = 150$ in Eq. (23). The permeability is estimated by Eq. (28) with an average relative error $\delta K/K = 40\%$.

The case of the drag coefficient, in Fig. 4, is quite different. We have reported there the compilation of values of C_F, plotted as a function of the CICC porosity, compared to the values predicted by Eq. (24). As already mentioned, the values derived from measured data are substantially lower than the expected range, by one order of magnitude.

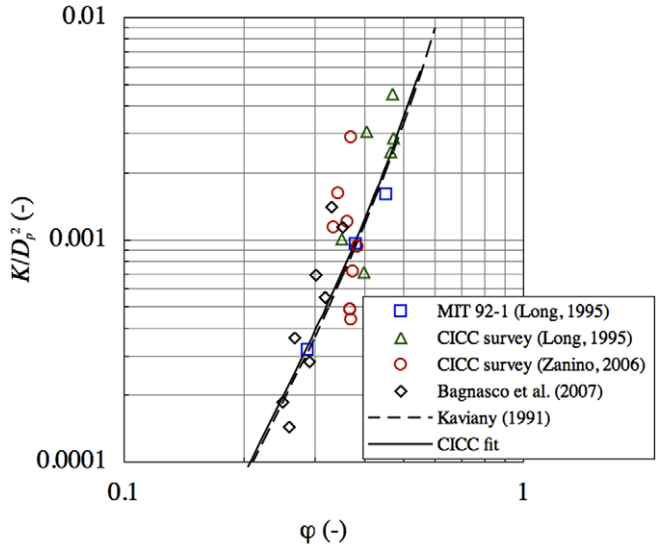

Fig. 3. Values of normalised permeability, plotted as a function of porosity, derived from the survey of Long [7], the survey of Zanino and Savoldi Richard [11], and the data deduced from measured pressure drop by Bagnasco et al. [24]. The measured data is compared to the theory of Kaviany [18] (Eq. (23)). The fit Eq. (28) is used for the prediction of CICC permeability as a function of porosity.

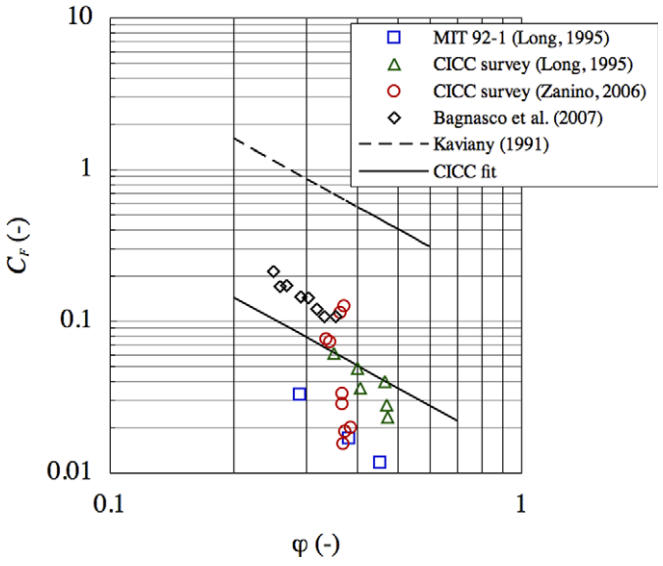

Fig. 4. Values of drag coefficient as a function of porosity, taken from the survey of Long [7], the survey of Zanino and Savoldi Richard [11], and the data deduced from measured pressure drop by Bagnasco et al. [24]. The prediction for packed bed of particles from Kaviany [18] (Eq. (24)) is reported for comparison. The data is fitted with Eq. (29).

An interesting feature is that the measured values seem to group in clusters that have an approximate dependency on the porosity of the type:

$$C_F = \frac{B}{\varphi^{3/2}} \tag{29}$$

which is consistent with the theoretical expectation of Eq. (24). The reasons for the clustering are so far unclear, although we suspect it to be associated with channeling and the presence of long parallel channels in the ordered structure of the twisted cable. This idea is supported by the observation that cables with identical structure, but different void fraction, have a drag coefficient dependence on the void fraction that follows closely Eq. (29). Although we recognise that this last effect is not properly parameterised, for the present we propose to use Eq. (29) with a value of $B = 0.013$ to give an order-of-magnitude estimate. This scaling, also reported in Fig. 4, results in a minimum residual with respect to the experimental data, and an average relative error $\delta C_F/C_F = 60\%$.

Given the above uncertainties, a simple error propagation analysis shows that at low Reynolds the overall uncertainty on the friction factor is $\delta f/f \approx \delta K/K$, corresponding to a relative error of 40% on the predicted friction factor. At high Reynolds the uncertainty on the friction factor is $\delta f/f \approx \delta K/2K + \delta C_F/C_F$, leading to an 80% relative error on the predicted friction factor. These values are marginally better or comparable to those quoted for the empirical fit of Eq. (21) [9], but the obvious advantage in this case is that the prediction is based on an established theory.

5. Effective conductivity and thermal dispersion

The effective thermal conductivity appearing in Eq. (11) results from two contributions: the molecular conductivity, and heat transfer due to mixing at the scale of the pores induced by vigourous convection. To clarify the second process, which is also called *thermal dispersion*, we can picture fluid elements starting at a distance from each other, and flowing in different channels. Because of the tortuosity of the channels, the fluid elements do not remain at the same distance apart along the flow path, and at some locations they can mix. The net effect is a two-ways macroscopic transport of mass that promotes mixing of fluid over distances much larger than the molecular length. In the presence of temperature gradients, this effect also results in heat transfer that, depending on the flow conditions, can be largely in excess of molecular diffusion.

An accurate description of thermal dispersion is a complex mathematical and physical matter. We consider here the case of isotropic medium and 1-D flow, and we limit ourselves to simple approximations for the effective longitudinal and transverse thermal conductivity that are obtained for beds of uniform spheres of diameter D_p. A suitable expression for the effective conductivity in the direction of the flow, is [6]:

$$k_L = \begin{cases} k_F & \text{for } Pe_\varphi \ll 1 \\ \frac{1}{1-\varphi}\frac{2B_L}{\pi} Pe_\varphi k_F & \text{for } Pe_\varphi \gg 1 \end{cases} \tag{30}$$

Above, k_F is the fluid molecular conductivity, and $B_L = 1.75$ is a constant determined empirically.

In the direction transverse to the flow, the effective thermal conductivity has been derived theoretically and experimentally, leading to several expressions depending on the

approach taken. The simplest expression was obtained correlating experimental data:

$$k_T = \begin{cases} k_F & \text{for } Pe_\varphi \ll 1 \\ k_F C_T Pe_\varphi & \text{for } Pe_\varphi \gg 1 \end{cases} \quad (31)$$

where C_T is a constant (empirically, $C_T = 0.09\ldots0.1$). The above equation was obtained as a fit to data. Hsu and Cheng [25] have provided a theoretical support for the asymptotic limit at high Peclet number. They have used volume averaging of the flow and temperature deviations from mean values, and have obtained the following expression:

$$k_T \approx k_F D_T \frac{1-\varphi}{\varphi} Pe_\varphi \quad (32)$$

where the value of the constant D_T is also determined experimentally. Eqs. (31) and (32) give comparable results for a value $D_T = 0.04$.

An alternative approach was followed by Bo-Ming and Jian-Hua [26], who used a fractal model to describe the tortuosity of the flow in a porous medium. Defining the ratio of the straight distance L_s travelled by a particle (the distance of a coherent macroscopic motion) to the size of the pore λ_{min} (the smallest scale of the movement), and the fractal dimension of the tortuous path δ (where $1 < \delta < 2$) they found that:

$$\delta = 1 + \frac{\ln\left(1+\sqrt{1-\varphi}\right)}{\ln(L_s/\lambda_{min})} \quad (33)$$

and that the effective transverse conductivity at high Peclet is given by:

$$k_T \approx k_F E_T \frac{1}{\varphi}\left[\delta\left(\frac{L_s}{\lambda_{min}}\right)^{\delta-1} - 1\right] Pe_\varphi \quad (34)$$

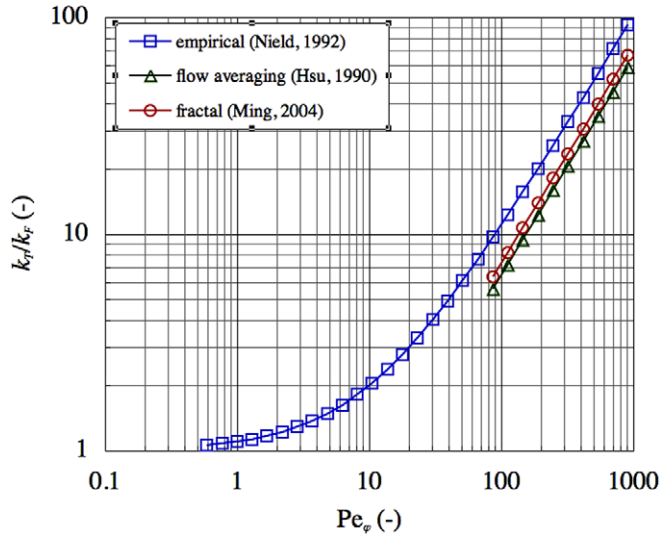

Fig. 5. Ratio of effective transverse thermal conductivity to fluid thermal conductivity, predicted by different theories listed in the text, and plotted as a function of Peclet number. The enhancement due to thermal dispersion is significant at seepage Peclet larger than 10.

where the constant E_T is based on experimental data. Taking the recommended ratio of $L_s/\lambda_{min} = 1000$, a value $E_T = 0.03$ yields consistent results to the work reported above.

Fig. 5 shows the dependencies of the ratio between the effective transverse thermal conductivity and the fluid thermal conductivity, obtained using the above models, as a function of the Peclet number. In the typical range of Peclet numbers of the above conditions (100–500) the enhancement factor is of the order of 10–50. This is a large factor, that contributes significantly to making the temperature in the cross section of a CICC uniform, which is an advantage from the point of view of operation of the cable.

6. Heat transfer in a CICC

Heat transfer is the second topic of practical interest in the design of a CICC. The main motivation is that the temperature of the strands shall be maintained as uniform and as close as possible to that of the coolant under any operating condition to maximise the superconductor margin with respect to critical conditions. In a porous medium, heat transfer depends on the total flow, on the thermodynamic state of the fluid, and, most important, on the geometry and size of the pores, affecting the flow pattern. The topic of heat transfer in porous media is by itself a vast subject of research, with considerable experimental difficulties. Here we take a simpler approach, distinguishing among the internal heat transfer coefficient h_{int} that governs heat exchange between the solid phase to the fluid phase at the pore level (i.e., strand to coolant), and an external heat transfer coefficient h_{ext} that governs the heat exchange from the boundary of the flow (walls, free boundaries) to the flow bulk.

Before we start the discussion, we remark that so far these two heat transfer mechanisms have been treated in a similar manner, using classical correlations for forced convection such as that of Dittus–Boelter [13]:

$$Nu = \frac{hD_h}{k_F} = 0.023 Re^{0.8} Pr^{1/3} \quad (35)$$

with various modifications to adapt it to the range of temperature and transient conditions [27–30]. The only exceptions are the studies of Long and Renard on the heat transfer at the interface between the coolant in the cable and the free flow in the cooling space in an ITER type conductor of the type discussed earlier.

6.1. Internal heat transfer coefficient

Several, specific correlations have been established for different types of porous medium and specific values of the void fraction. Some examples have been collected from selected works of Whitaker [31], Wakao and Kaguei [32], Zukauskas [33], the review of Achenbach [22], and Bird et al. [13]. We show in Fig. 6 the comparison of the predictions of the above correlations over a wide range of Rey-

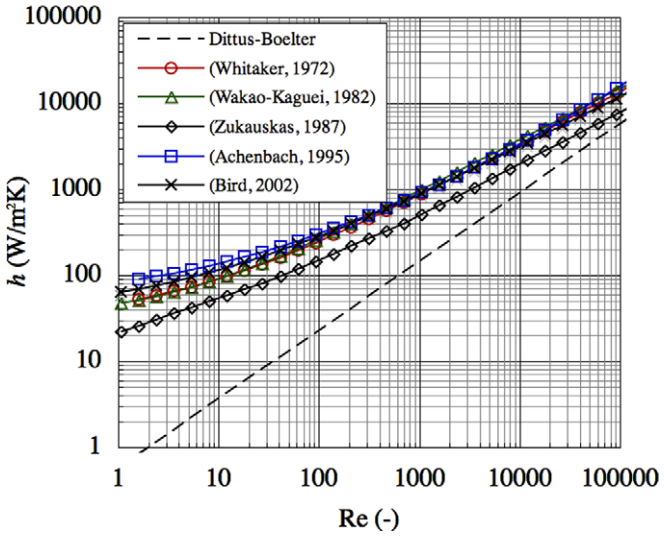

Fig. 6. Internal heat transfer coefficient (strand-helium) computed from the correlation of Dittus–Boelter (Eq. (35)), as compared to the prediction of the correlation proposed, from Achenbach [22] (Eq. (37)). Also reported for comparison the values obtained using the correlations of Bird et al. [13], Whitaker [31], Wakao and Kaguei [32], and Zukauskas [33].

nolds number, as compared to the result of the Dittus–Boelter correlation Eq. (35). The correlations from the above references need to be reworked considerably to express them in terms of the hydraulic diameter and Reynolds number of the flow as defined in Eqs. (4) and (17).

For sufficiently large Reynolds ($Re > 100$), the correlations reported agree well with each other and predict a heat transfer coefficient much higher than that of the Dittus–Boelter correlation. At low Reynolds number, as discussed by Achenbach [22], other heat transfer mechanisms can become significant. This results in a large uncertainty on the value of the forced convection heat transfer coefficient in this range of Re, and the question whether the Nusselt number has a lower limit is so far undecided. For this regime Achenbach recommends using a lower limit for the Nusselt number around a sphere [22]:

$$\frac{h_{\mathrm{int}} D_{\mathrm{particle}}}{k_{\mathrm{F}}} = 2 \tag{36}$$

We have combined the above limit to the correlation from [13] as follows:

$$\frac{h_{\mathrm{int}} D_{\mathrm{h}}}{k_{\mathrm{F}}} = \left[\frac{4}{3}\frac{\varphi}{1-\varphi} + \varphi\left(1.671 Re^{1/3} + 0.668 Re^{0.619}\right)\right] Pr^{1/3} \tag{37}$$

that has the advantage of simplicity and produces results in the consistent with those from most references quoted above.

As a final comment to the above discussion, and for the sake of completeness, we observe that the values of the internal heat transfer coefficient reported in the literature show a great variability. Achenbach justifies the spread with the difficulty of controlling the sample geometry and the experimental conditions. At any rate, values up to an order of magnitude higher are given for tightly packed or sintered particle beds and foams, see as an example [34,35].

6.2. External heat transfer coefficient

The external heat transfer coefficient depends on the flow in the porous media as well as on that of the external boundary (pipe wall, channel boundary) where the heat transfer takes place. We consider here the case of a pipe of diameter D_{pipe} which is a case study of practical interest for the CICC geometry considered.

Nield [6] proposes in this case to use standard correlations for forced convection, modified as follows to take into account the effect of thermal dispersion:

$$\frac{h^{\mathrm{porous}}}{h^{\mathrm{free}}} \approx \frac{k_{\mathrm{T}}}{k_{\mathrm{F}}} \tag{38}$$

where h^{porous} indicates the heat transfer coefficient in the porous flow, and h^{free} is the heat transfer coefficient as would be obtained in the same configuration, but considering free flow under the same conditions. Their ratio is proportional of the ratio of the effective thermal conductivity of the porous medium to the molecular fluid conductivity, which, as discussed earlier, can be large at large Peclet number. In practice, we can estimate the external heat transfer as follows:

$$\frac{h_{\mathrm{ext}} D_{\mathrm{pipe}}}{k_{\mathrm{T}}} = 8 + 0.023 Re_{\mathrm{pipe}}^{0.8} Pr^{1/3} \tag{39}$$

where we have indicated with Re_{pipe} the Reynolds number of the flow referred to the pipe diameter, or:

$$Re_{\mathrm{pipe}} = \frac{\rho v D_{\mathrm{pipe}}}{\mu} \tag{40}$$

In the expression above, Eq. (39), we have introduced a lower limit to the pipe Nusselt number of 8, as would be obtained for laminar flow under constant heat flux.

We expect the above approximation to hold as long as the thermal boundary layer is large when compared to the length scale of mass exchange between pores, i.e., such that thermal dispersion is effective within the thermal boundary layer. This will obviously be true at low Reynolds number. At high Reynolds number, an alternative to Eq. (39) is the following correlation for pipes filled with packed beds of sphere proposed by Achenbach [22]:

$$h_{\mathrm{wall}} = \frac{k_{\mathrm{F}}}{D_{\mathrm{p}}}\left(1 - \frac{D_{\mathrm{particle}}}{D_{\mathrm{pipe}}}\right) Re_{\varphi}^{0.61} Pr^{1/3} \tag{41}$$

that is valid for $Re > 100$.

We report in Fig. 7 the comparison of the heat transfer coefficient obtained with a Dittus–Boelter correlation with a lower limit of 8 on the Nusselt number and the two correlations Eqs. (39) and (41), evaluated for a CICC with a cable made with strands of 0.8 mm diameter at 35% void fraction. We also report for comparison values obtained with the correlations proposed by Yagi and Wakao [36]

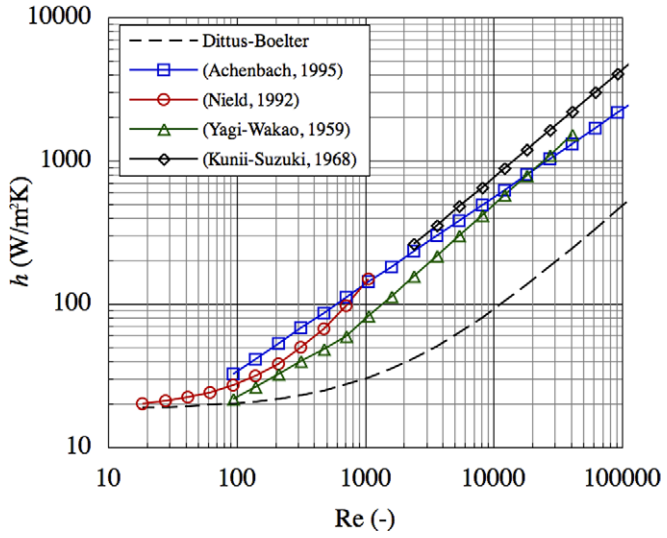

Fig. 7. External heat transfer coefficient (conduit-helium) computed from the correlation of Dittus–Boelter (Eq. (35)), as compared to the prediction obtained using the method proposed by Nield [6] (Eq. (39)) for $Re < 1000$ and Achenbach [22] (Eq. (41)) for $Re > 1000$. Also reported for comparison the values obtained from the correlations of Yagi and Wakao [36] and Kunii and Suzuki [37].

and Kunii and Suzuki [37] (as reported by Dixon and Cresswell [38]). As for the internal heat transfer, the porous media correlations are much higher than the heat transfer predicted in the case of free flow, by nearly a factor 10 in the range of Re of practical interest, $Re > 1000$. The two porous media correlations discussed above give similar results in the range of $100 < Re < 1000$, where we expect the transition from a regime dominated by dispersion in the thermal boundary layer to a regime dominated by local turbulence. For practical use we propose to use Eq. (39) up to $Re = 1000$, and Eq. (41) beyond.

7. Boundary effects

So far we have considered in the discussion a uniform and unbounded medium. This is not appropriate in the case of the superconducting cable considered. While the medium is indeed unbounded in longitudinal direction, and can be considered unbounded (periodic) along the perimeter, it has discontinuities in radial direction. Taking the example of the ITER conductor of Fig. 1 (bottom, right), the discontinuities are the cooling channel at the inner radius and the jacket at the outer radius. As discussed in [6] and [25], this causes a local change of porosity which results in channeling effects (increased local massflow at the two boundaries) and a modification of the mixing properties discussed above.

The effective porosity at the wall can be as large as twice the nominal value. The dimension affected is of the order of a fifth of the characteristic size of the solid phase, i.e., the strand radius. The flow in this region is much less constricted (channeling), and the local seepage velocity is increased with respect to the average value. In a CICC the size of the strand is only 10–50 times smaller than the cable size, and channeling can contribute to a large reduction of the pressure drop. This effect is surely one of the reasons why the pressure drop in a CICC is much smaller than expected for a bed of packed spheres of equivalent diameter.

A modification of the local value of the porosity also leads to a change in the local thermal dispersion and heat transfer. In fact, following Hsu and Cheng [25], thermal dispersion is modified over a length of the same scale as the characteristic dimension of the solid phase.

The combined effect of channeling and modified heat transfer at the boundary of the cable results in steep temperature gradients and limited mixing in the cable cross section, as observed experimentally by Bruzzone et al. [39]. Being aware of these effects is important, to put in the proper perspective the predictive value of the correlations discussed above.

8. Analysis of thermal dispersion in a CICC sample

The analysis of experimental data collected during the cryogenic tests of the Low-Cost Joint ITER conductor sample [40] provides a good example of application of the analogy to porous media discussed in this paper. The experiment consists in the measurement of the temperature distribution downstream of a local heater placed in a heavily instrumented CICC. The CICC contains a cable made of 864 strands, wound around a central spiral. The inner diameter of the spiral is 9.4 mm, while the outer diameter of the cable is 36 mm. The cable is inserted in a 316LN pipe with an outer diameter of 39.5 mm. The heater, a strip 8 mm wide and 38 mm long, is glued to the SS pipe and covers a small extent compared to the cable size. The temperature is measured at three longitudinal locations along the CICC, placed at 140 mm, 640 mm, and 1120 mm from the heater. Each location is equipped with six thermometers that record the azimuthal temperature distribution in the cross section and a thermometer placed in he center of the spiral, measuring the temperature of the helium flowing in the central space. The measurement runs were performed at an initial temperature of 4.5 K, pressure of 10 bar, and in a range of total massflow from 2 to 8 g/s. A cross section of the CICC equipped with the thermometers mounted in a ring around the jacket is shown in Fig. 8. A summary of the main cable geometry data and operating conditions is reported in Table 1. Further details on the experiment can be found elsewhere [40].

We have analysed the steady-state temperature profiles induced by the heater as a function of the massflow of coolant in the CICC. The azimuthal temperature profile, i.e. measured along the cable perimeter in each of the three cross sections, was analysed in Fourier series to obtain a modal decomposition of the temperature distribution in the cable. A simple analytical model was developed for the dependence of the lowest order mode of the temperature distribution on the longitudinal position. The model

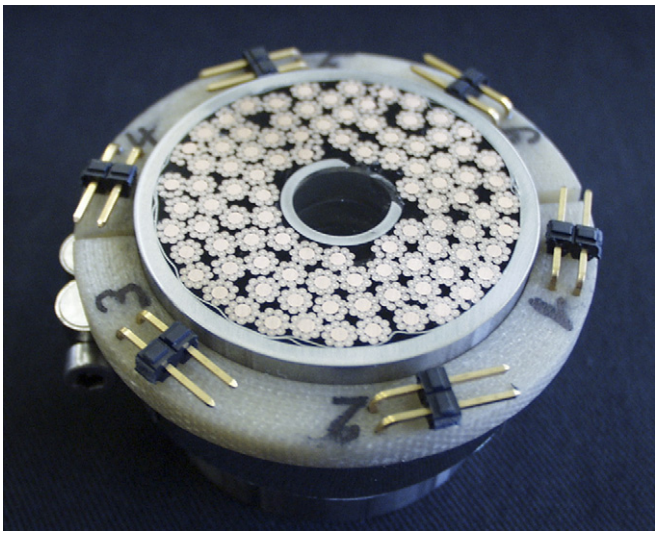

Fig. 8. Cross section of the LCJ dual channel cable-in-conduit conductor with the sensor ring applied on its jacket [40].

Table 1
Cable geometry and operating conditions for the heat transfer experiment performed on the Low-Cost Joint ITER CICC sample, from Ref. [40]

Conductor outer diameter	(mm)	39.50
Cable space diameter	(mm)	35.95
Strand diameter (D_{strand})	(mm)	0.73
Number of strands	(–)	864
Cosine of the average cabling angle ($\cos\theta$)	(–)	0.96
Spiral inner diameter	(mm)	9.40
Spiral outer diameter	(mm)	11.40
Spiral perforation	(%)	25
Wrap thickness	(mm)	0.10
Total helium in bundle (A_F)	(mm^2)	349.8
Helium in central channel (hole)	(mm^2)	69.4
Hydraulic diameter of bundle (D_h)	(mm)	0.75
Hydraulic diameter of hole	(mm)	11.40
Void fraction of bundle (φ)	(%)	38.3
Inlet temperature	(K)	4.5
Inlet pressure	(bar)	10
Massflow	(g/s)	2...8

is based on parallel cooling channels exchanging heat through a fictive heat transfer coefficient that represents the transverse thermal resistance of the fluid, estimated as:

$$h_{transverse} = \frac{k_T}{t} \tag{42}$$

where t is the characteristic length of the heat exchange between the parallel channels, of the order of 10 mm in our specific case. The heat transfer coefficient $h_{transverse}$ is determined fitting the measured dependence of the temperature profiles. Using Eq. (42) it is then possible to infer the value of the effective transverse thermal conductivity. The results of this analysis are reported in Fig. 9, where we have plotted for comparison the estimates of k_T obtained with Eqs. (31), (32), and (34). In the comparison we have neglected the contribution of thermal conduction in the solid phase, which is justified by the presence of a significant thermal

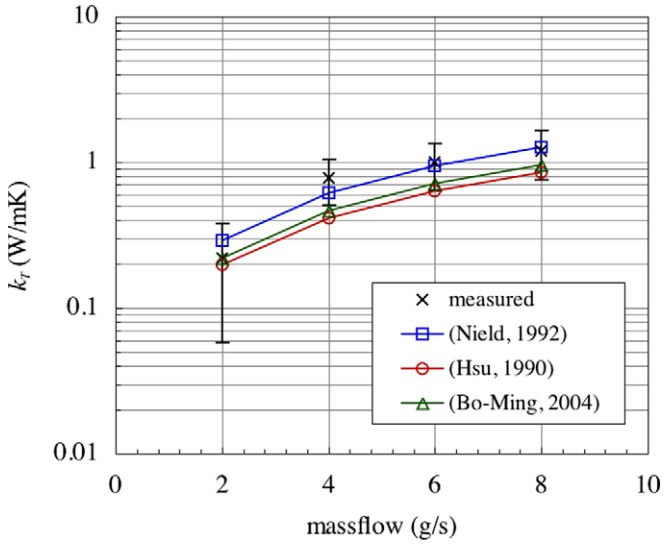

Fig. 9. Comparison of effective fluid transverse thermal conductivity as obtained from the analysis of the steady-state temperature distribution in the LCJ sample, and the theory of Nield (Eq. (31)) [6], Hsu and Cheng (Eq. (32)) [25], and Bo-Ming and Jian-Hua (Eq. (34)) [26].

resistance at the fluid–solid interface. The agreement between the measured and expected effective thermal conductivity is satisfactory, and shows that thermal dispersion can have a major role in heat transport within the cross section of a CICC.

9. Conclusions

For the prediction and interpretation of pressure drop and heat transfer we propose to use an analogy between the cable in a Cable-in-Conduit superconductor and a porous medium of the same porosity and equivalent geometry. The analogy can shed new light on the results accumulated so far, provide a new view point for their interpretation, a useful tool for prediction, and guidelines for experimental work.

We have shown in particular that porous media correlations can be used to fit existing CICC pressure drop data. We have provided scaling models for the prediction of permeability and drag coefficient as a function of the void fraction and the strand diameter. We believe that channeling, associated with the multi-stage cabling pattern of the cable, is significant. A better characterisation of this effect is required to improve the prediction capability of the pressure drop correlation.

Based on the porous medium analogy, the expected heat transfer in the CICC geometry is much larger than the values used to date, that are based on adapted pipe correlations. The expected thermal dispersion has been verified in a dedicated experiment, and the result found is consistent with the expected range of convective enhancement of the fluid thermal conduction coefficient.

This approach appears promising, but before proceeding any further with theory and analysis, it is mandatory to validate the concept by means of dedicated experiments

on the details of the cable hydraulic and thermal properties. As the scalings and correlations discussed in this paper are given in terms of physical parameters such as the void fraction or the cable strand, it should be relatively easy to design experiments that test parametrically the expected functional dependencies and extend the existing database.

Acknowledgements

We are indebted to M. Bagnasco and P. Bruzzone of EPFL/CRPP (Villigen, Switzerland) and M. Lewandowska (Szczecin University of Technology, Szczecin, Poland) for the pressure drop data they provided and analysed, and the useful discussions in the determination of permeability and drag.

References

[1] M.O. Hoenig, D.B. Montgomery, Dense supercritical helium cooled superconductors for large high field stabilized magnets, IEEE Trans. Mag. 11 (2) (1975) 569–572.
[2] M.O. Hoenig, Y. Iwasa, D.B. Montgomery, Supercritical-helium cooled bundle conductors and their application to large superconducting magnets, in: Proceedings of the Fifth Magn. Tech. Conf., Frascati, 1975, pp. 519–521.
[3] J.L. Duchateau, Development of high-current high-field conductors in Europe for fusion application, Supercond. Sci. Technol. 15 (R17–R29) (2002).
[4] C. Sborchia et al., Manufacture and testing of the W7-X superconducting magnets, IEEE Trans. Appl. Sup. 16 (2) (2006) 848–851.
[5] L. Bottura, Cable-in-Conduit, chapter B-3.4 of handbook of applied superconductivity, in: B. Seeber (Ed.), Institute of Physics Publishing, Bristol, 1998, pp. 151–171.
[6] D.A. Nield, A. Bejan, Convection in Porous Media, third ed., Springer-Verlag, New York, 2006.
[7] A.E. Long, Transverse heat transfer in a cable-in-conduit conductor with central cooling channel, M.Sc. Thesis, MIT, Cambridge, MA, 1995.
[8] B. Renard, Thermo-hydraulic bevahiour of dual channel superconducting Cable-in-Conduit conductors for ITER, Ph.D. Thesis, Universite de Provence, Marseille-F, 1995.
[9] H. Katheder, Optimum thermohydraulic operation regime for cable in conduit superconductors (CICS), Cryogenics 34 (Suppl. 1) (1994) 595–598.
[10] Q. Wang, P. Weng, M. He, Simulation of quench for the Cable-in-Conduit-Conductor in HT-7U superconducting Tokamak magnets using porous medium model, Cryogenics 44 (2004) 81–92.
[11] R. Zanino, L. Savoldi Richard, A review of thermal-hydraulic issues in ITER Cable-in-Conduit conductors, Cryogenics 46 (2006) 541–555.
[12] L. Bottura, Stability, protection and AC loss of Cable-in-Conduit conductors – A designer's approach, Fusion Eng. Des. 20 (1993) 351–362.
[13] R.B. Bird, W.E. Stewart, E.N. Lightfoot, Transport Phenomena, John Wiley & Sons, 2002.
[14] L. Dresner, Stability of Superconductors, Plenum Press, 1995.
[15] A. Shajii, J.P. Freidberg, Theory of low Mach number compressible flow in a channel, J. Fluid Mech. 313 (1996) 131–145.
[16] J.C. Ward, Turbulent flow in porous media, ASCE J. Hydraul. Div. 90 (HY5) (1964) 1–12.
[17] L. Dresner, J.W. Lue, Design of force-cooled conductors for large fusion magnets, in: Proceedings of the Seventh Symp. Eng. Prob. Fus. Res., vol. I, 1977, pp. 703–709.
[18] M. Kaviany, Principles of Heat Transfer in Porous Media, Springer Verlag, New York, 1991.
[19] A. Koponen, D. Kandhai, E. Hellin, M. Alava, A. Hoekstra, M. Kataja, K. Niskanen, P. Sloot, J. Timonen, Permeability of three-dimensional random fiber webs, Phys. Rev. Lett. 80 (4) (1998) 716–719.
[20] V.V. Calmidi, Transport phenomena in high porosity fibrous metal foams, Ph.D. Thesis, University of Colorado, 1998.
[21] S. Ergun, Fluid flow through packed columns, Chem. Eng. Prog. 48 (1952) 89–94.
[22] E. Achenbach, Heat and flow characteristics of packed beds, Exp. Therm. Fluid Sci. 10 (1995) 17–27.
[23] W.T. Wu, J.F. Liu, W.H. Hsieh, Measurement and correlation of hydraulic resistance of flow through woven metal screens, Int. J. Heat Mass Transfer 48 (2005) 3008–3017.
[24] M. Bagnasco, L. Bottura, P. Bruzzone, M. Lewandowska, C. Marinucci, F. Staehli, Pressure drop of Cable-in-Conduit conductors with different void fraction, Transactions of the Cryogenic Engineering Conference, CEC, Chattanooga, TN, July 16–20, 2007. Advances in Cryogenic Engineering, vol. 53, AIP Conference Proceedings.
[25] C.T. Hsu, P. Cheng, Thermal dispersion in a porous medium, Int. J. Heat Mass Transfer 33 (8) (1990) 1587–1597.
[26] Y. Bo-Ming, L. Jian-Hua, A fractal model for the transverse thermal dispersion conductivity in porous media, Chin. Phys. Lett. 21 (1) (2004) 117–120.
[27] P.J. Giarratano, V.D. Arp, R.V. Smith, Forced convection heat transfer to supercritical helium, Cryogenics 11 (1971) 385–393.
[28] L.A. Yaskin, M.C. Jones, et al., A correlation for heat transfer to supercritical helium in turbulent flow in small channels, Cryogenics 17 (1977) 549–552.
[29] P.J. Giarratano, W.G. Steward, Transient forced convection heat transfer to helium during a step in heat flux, Trans. ASME 105 (1983) 350–357.
[30] W.B. Bloem, Transient heat transfer to a forced flow of supercritical helium at 4.2 K, Cryogenics 26 (1986) 300–308.
[31] S. Whitaker, Forced convection heat transfer correlations for flow in pipes, past flat plates, single cylinders, single spheres, and for flow in packed beds and tube bundles, AIChE J. 18 (2) (1972) 361–371.
[32] N. Wakao, S. Kaguei, Heat and Mass Transfer in Packed Beds, Gordon and Breach Science, New York, 1982.
[33] A.A. Zukauskas, Convective heat transfer in cross-flow, in: S. Kakac, R.K. Shah, W. Aung (Eds.), Handbook of Single-Phase Convective Heat Transfer, Wiley, New York, 1987.
[34] K.K. Kar, A. Dybbs, Internal heat transfer coefficients of porous metals, in: J.V. Beck, L.S. Yao (Eds.), Heat Transfer in Porous Media, HTD-22, ASME, 1982.
[35] A.R. Raffray, J.E. Pulsifer, MERLOT: A model for flow and heat transfer through porous media for high heat flux applications, Internal Report UCSD-ENG-087, University of California, 2001.
[36] S. Yagi, H. Wakao, Heat and mass transfer from wall to fluid in packed beds, AIChE J. 5 (1959) 79.
[37] D. Kunii, M. Suzuki, Paper presented to Symposium on Heat and Mass Transfer, Minsk, 1968.
[38] A.G. Dixon, D.L. Cresswell, Theoretical Prediction of effective heat transfer parameters in packed beds, AIChE J. 25 (4) (1979) 663–676.
[39] P. Bruzzone, A.M. Fuchs, G. Vecsey, E. Zapretelina, Test results for the high field conductor of the ITER central solenoid model coil, Adv. Cryogen. Eng. 45 (2000) 729–736.
[40] C. Marinucci, L. Bottura, P. Bruzzone, B. Stepanov, Analysis of the transverse heat transfer coefficients in a dual channel ITER-type Cable-in-Conduit conductor, Cryogenics (in press).